North Pacific Variability and Climate Patterns During the 1997-98 ENSO Event

Kenneth S. Casey*, COMNAVMETOCCOM Chair in Remote Sensing, United States Naval Academy and David Adamec, NASA Goddard Space Flight Center

1. ABSTRACT

Singular Value Decomposition (SVD) and Empirical Orthogonal Function (EOF) analyses of AVHRR Pathfinder and TOPEX data are used to investigate the coupled sea surface temperature (SST) and sea surface height (SSH) variability in the Equatorial and North Pacific before and during the 1997-98 El Niño - Southern Oscillation (ENSO) event. This coupled variability is related to the dominant modes of Pacific climate variability and these relationships are explored by correlating the SVD/EOF results with the Southern Oscillation Index (SOI) and climate pattern indices for the Pacific North American (PNA) pattern and the Pacific Decadal Oscillation (PDO). Eddy-mean flow interactions are identified during the 1997-98 ENSO and compared to characterizations of the 1993-94 and 1995-96 periods. These comparisons identify changes in the instability mechanisms throughout the time period.

Strong correlations between the tropical and extra-tropical SST/SSH variability and the SOI are identified at a lag of zero months, indicating the dominance of the interannual ENSO mode on Pacific climate variability. These correlations are significant at the 95% confidence level. Somewhat weaker but still statistically significant correlations with the PNA pattern are also observed with the PNA pattern trailing by four months. The PNA pattern correlations represent a longer time scale interdecadal mode of variability. The relationship between the SST/SSH variability and the PDO pattern is not significant, however.

Excluding the tropics from the SVD analysis permits a more detailed examination of the extra-tropical North Pacific variability. Correlations between the extra-tropical SST/SSH variability and the SOI weaken but remain significant. A lag of eight months with SOI leading also appears, suggesting that the ENSO signal takes at least several months to impact the higher-latitude SST/SSH relationships. Correlations between the SST/SSH modes and the PNA index remain near the levels they had when the tropical Pacific was included in the analysis and the time lag decreases to one month with the PNA leading, suggesting the PNA and extra-tropical North Pacific oceanic variability are more closely in phase with one another. Again, correlations with the PDO pattern remain below the 95% confidence level.

2. INTRODUCTION

Because of the recent availability of numerous in situ and remotely-sensed data sets, the strong 1997-98 El Niño was better observed than any previous phase of the El Niño Southern Oscillation (ENSO). The quantity and variety of available data have allowed this climate pattern to be studied from numerous perspectives. Using Special Sensor Microwave Imager (SSM/I) satellite wind observations and other data sources, Yu and Rienecker (1998) found that anomalous extra-tropical winds associated with the Madden-Julian Oscillation intruded over the western equatorial Pacific and acted to enhance the westerly wind bursts likely responsible for triggering the El Niño event. Chavez et al. (1998) found a close coupling between primary production and the El Niño-related thermocline variations using bio-optical instrumentation on the Tropical Atmosphere Ocean (TAO) array. Several satellite sensors were used by Chandra et al. (1998) to examine the effect of the strong El Niño on tropospheric ozone and water vapor. They found that the eastward shift in tropical Pacific convection was associated with decreasing tropospheric column ozone levels in the eastern Pacific and increasing levels in the west. The opposite pattern was found for water vapor: decreasing levels in the west resulting from suppressed convection and increasing levels in the east resulting from increased convection. McPhaden (1999) examined data from the TAO array in the equatorial Pacific to describe the physical processes which influenced the formation and evolution of the El Niño. That study suggested that the strength and rapid development of the 1997-98 El Niño were related to intraseasonal atmospheric oscillations and that its rapid termination could be attributed to low-frequency oceanic processes that elevated the central and Eastern Pacific thermocline and an abrupt intensification of the trade winds.

The present study takes an oceanic perspective to investigate North Pacific sea surface temperature (SST) and sea surface height (SSH) variability during 1997-98, extending the work of Casey and Adamec (1999) which examined the 1993-96 period. The coupled SST-SSH variability is investigated using Pathfinder AVHRR and TOPEX data and related to the dominant modes of Pacific climate variability. These relationships are studied by correlating the results of a singular value decomposition (SVD) analysis with the Southern Oscillation Index (SOI) and climate pattern indices for the Pacific-North American (PNA) pattern and the Pacific Decadal Oscillation (PDO). Eddy-mean flow interactions are also characterized during the 1997-98 El Niño and compared to the 1993-94 and 1995-96 periods examined in Casey and Adamec (1999).

References

Casey, K. S. and D. Adamec (1999). Sea surface temperature and sea surface height variability in the North Pacific Ocean from 1993-1996. *Journal of Geophysical Research*. submitted.

Chandra, S., J. Ziemke, W. Min, and W. Read (1998). Effects of 1997-1998 el niño on tropospheric ozone and water vapor. *Geophysical Research Letters 25*, 3867–3870.

Chavez, F. P., P. G. Strutton, and M. J. McPhaden (1998). Biological-physical coupling in the central equatorial Pacific during the onset of the 1997-98 el niño. *Geophysical Research Letters 25*, 3543–3546.

McPhaden, M. J. (1999). Genesis and evolution of the 1997-98 el niño. *Science 283*, 950–954.

Yu, L. and M. M. Rienecker (1998). Evidence of and extratropical atmospheric influence during the onset of the 1997-98 el niño. *Geophysical Research Letters 25*, 3537–3540.

3. METHODS

- TOPEX/Poseidon Generation B Merged Geophysical Data Records for cycles 11 through 231 (1993-1998) were used to create mean SSH fields for each calendar month. Anomaly fields were then created for each cycle by subtracting the corresponding mean monthly field, averaging along-track, and optimally interpolating to a one-degree grid centered on the central day of the cycle. The one-degree grid is then averaged onto a two-degree grid.
- Mean SST fields from Version 4 of the AVHRR Pathfinder data set are created on a one-degree grid for each roughly ten-day cycle period from 1993-1998. Anomaly fields are generated by subtracting monthly means, and the resulting anomalies are then averaged onto a two-degree grid using the same technique applied to the SSH data. These two steps produce sets of temporally and spatially co-located SSH and SST anomaly fields for the Pacific Ocean between 10°S and 60°N.
- The time series of anomalies at each spatial location are de-meaned and normalized by dividing by their temporal standard deviations. An EOF analysis is conducted on each normalized field separately, and the SVD analysis is performed on the cross-covariance matrix of the two fields.
- Results of the EOF analysis are plotted as spatial variance maps and time series of expansion coefficients (not shown). Results of the SVD analysis are plotted as heterogeneous covariance maps and expansion coefficient time series (Figure 1).
- Lagged correlations between the time series of SVD expansion coefficients and the Southern Oscillation Index (SOI) and indices for the Pacific North American (PNA) pattern and the Pacific Decadal Oscillation (PDO) are computed (Figures 2 and 3).
- The tropics are excluded from the SVD analysis and the lagged correlations are again computed (Figures 4 and 5).
- The one-degree SSH and SST anomaly grids are used to calculate and compare the EKE levels (Figure 6), eddy heat flux convergence (Figures 7), downgradient eddy heat flux (Figure 8), and the sum of the barotropic conversion terms (Figure 9), during 1993-94, 1995-96, and 1997-98.

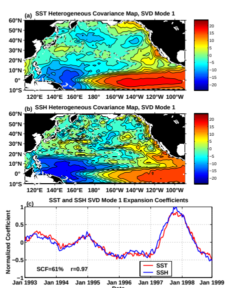

Figure 1. Heterogeneous covariance maps for first SVD mode for SST and SSH. The heterogeneous spatial patterns of the first SVD mode are shown for SST and SSH. The first three modes account for 61%, 20%, and 9% of the squared covariance of the two fields. The maps indicate how well the SST (SSH) anomaly patterns can be predicted from the SSH (SST) expansion coefficients for the given mode. The dashed line marks the zero contour and the contour interval is 3.0.

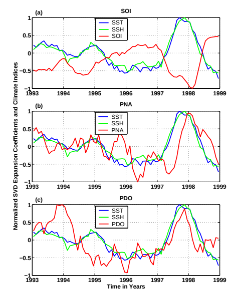

Figure 2. SVD Expansion Coefficients and Climate Indices The time series of first SVD mode expansion coefficients and the (a) SOI, (b) PNA index, and (c) PDO index. Gaps in the PNA index during each June and July have been replaced with a linearly interpolated value, each of the climate indices has been smoothed with a five-month running mean, and the SVD expansion coefficients have been interpolated to the monthly time steps of the climate indices.

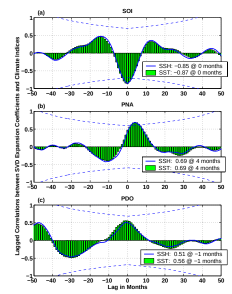

Figure 3. Lagged Correlations. Lagged correlations between the first SVD mode and the (a) SOI, (b) PNA index, and (c) PDO index. The SST (SSH) correlations are indicated by the bars (lines). The 95% confidence levels for SST are indicated by the dashed lines (SSH levels are similar and not shown). The maximum correlations and their lags in months are indicated. The climate index leads for negative lags, while SST/SSH lead for positive lags.

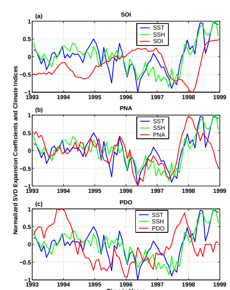

Figure 4. Extra-tropical SVD Expansion Coefficients and Climate Indices These correlations are similar to those in Figure 2, except the tropics have been excluded from this analysis, thereby limiting the domain to the extra-tropical North Pacific only.

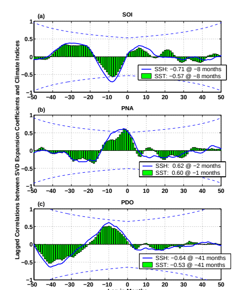

Figure 4. Extra-tropical Lagged Correlations. These lagged correlations are similar to those in Figure 3, except the tropics have been excluded from this analysis, thereby limiting the domain to the extra-tropical North Pacific only.

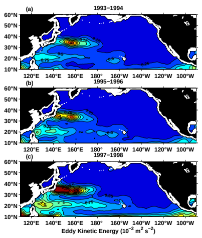

Figure 6. Eddy Kinetic Energy. The eddy kinetic energy for (a) 1993-94, (b) 1995-96, and (c) 1997-98. The contour interval is $0.25 \times 10^{-2} m^2 s^{-2}$.

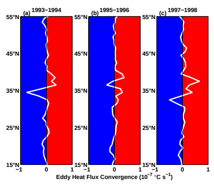

Figure 7. Eddy Heat Flux Convergence. The eddy heat flux convergence ($10^{-7} {}^{\circ}C s^{-1}$), zonally averaged to the dateline, for (a) 1993-94, (b) 1995-96, and (c) 1997-98.

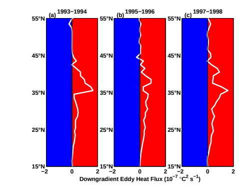

Figure 8. Downgradient Eddy Heat Flux. The downgradient eddy heat flux ($10^{-7} {}^{\circ}C^2 s^{-1}$), zonally averaged to the dateline, for (a) 1993-94, (b) 1995-96, and (c) 1997-98.

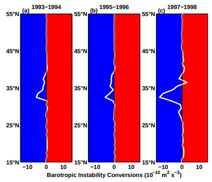

Figure 9. Sum of Barotropic Conversion Terms. The sum of the barotropic conversion terms ($10^{-10} m^2 s^{-3}$), zonally averaged to the dateline, for (a) 1993-94, (b) 1995-96, and (c) 1997-98.

4. SUMMARY

- The first EOF modes for SST and SSH individually show strong similarities and their expansion coefficients (not shown) are significantly correlated. This correlation provides justification for use of the SVD analysis to examine their coupled modes of variability. The SVD analysis identifies a strong ENSO-like pattern (Figure 1a,b) which broadly separates the six years into three periods: 1993-94, 1995-96, and 1997-98 (Figure 1c).
- Strong correlations between the tropical and extra-tropical SST/SSH variability and the SOI are identified at a lag of zero months, indicating the dominance of the ENSO mode on the coupled variability. Strong correlations are also observed with the PNA pattern trailing by four months. No significant correlation is observed with the PDO (Figures 2 and 3).
- Strong correlations with the SOI are still observed when examining only the extra-tropical SST/SSH variability, but the correlation weakens somewhat and a lag of eight months with the SOI leading appears (Figures 4 and 5). The PNA pattern is still strongly correlated, and the lag reduces to one month with the PNA leading. The extra-tropical SST/SSH variability is therefore more closely in phase with the PNA pattern than the ENSO pattern, whose influence takes about three seasons to reach the extra-tropics Again, no PDO correlation is observed.
- Examination of the eddy kinetic energy (Figure 6) indicates more vigorous eddy activity during the strong 1997-98 El Niño and the weak warm ENSO phase of 1993-94 than during the 1995-96 period. These relatively warm periods also experience greater baroclinic instability activity in the vicinity of the Kuroshio Extension, and all three periods have small levels of baroclinic instability in the vicinity of 20°N (Figures 7 and 8). Examination of the barotropic conversion terms reveals much greater barotropic instability activity in the Kuroshio Extension during the 1997-98 El Niño (Figure 9).

*Contact Information: United States Naval Academy, Dept. of Oceanography, 572M Holloway Road, Annapolis MD 21402, USA. casey@usna.edu, http://mohawk.gsfc.nasa.gov/˜casey